ELSEVIER

Chemical Engineering Journal 134 (2007) 138–144

Chemical Engineering Journal

www.elsevier.com/locate/cej

Kinetic evaluation of carbon formation in a membrane reactor for methane reforming

Marisa N. Pedernera, Juliana Piña, Daniel O. Borio *

Department of Chemical Engineering-PLAPIQUI, Universidad Nacional del Sur-CONICET, Camino La Carrindanga, Km 7, 8000 Bahía Blanca, Argentina

Abstract

In the present work, the effect of hydrogen removal on carbon formation in a membrane reactor (with nickel supported catalyst) for steam and CO_2 methane reforming is analyzed. The steady-state operation of the membrane reactor is described by means of a one-dimensional, heterogeneous, non-isothermal mathematical model. The carbon formation is kinetically evaluated through expressions reported in the literature. Higher CO_2 contents in the feed stream or operating temperatures increase the risk of carbon formation in both, the membrane and conventional fixed bed reactors. Moreover, for a given feed composition and tube-wall temperature profile, the tendency to carbon deposition is promoted by hydrogen removal and increases as the percentage of hydrogen removed is augmented (for example, by a diminution of the Pd membrane thickness). The proposed model is a useful tool to predict the position where carbon formation is expected in the conventional and membrane reactors for methane reforming, not only along the catalyst tube but also within the Ni particle.

Keywords: Methane reforming; Membrane reactor; Carbon formation; Reactor modeling

1. Introduction

Methane steam reforming is one of the most important processes for the production of hydrogen and synthesis gas. It may be represented by the following system of reversible reactions:

$$CH_4 + H_2O \leftrightarrow CO + 3H_2, \quad \Delta H^{\circ}_{298\,K} = 206\,kJ/mol \tag{1}$$

$$CO + H_2O \leftrightarrow CO_2 + H_2, \quad \Delta H^{\circ}_{298\,K} = -41\,kJ/mol \tag{2}$$

$$CH_4 + 2H_2O \leftrightarrow CO_2 + 4H_2, \quad \Delta H^{\circ}_{298\,K} = 165\,kJ/mol \tag{3}$$

Traditionally, this process is carried out in a furnace containing tubes packed with a supported nickel catalyst, which operates at high temperatures (around 800 °C), pressures between 1.6 and 4.1 MPa and steam to methane ratios within the range 2–4.

Deactivation of nickel catalysts by carbon formation is a significant problem in methane reforming caused by fouling of the Ni surface, blockage of the pores of the catalytic particle and disintegration of the support material [1]. Thermodynamically, the most probable reactions for carbon formation are the following equations:

$$\text{CH}_4 \text{ cracking} \qquad CH_4 \leftrightarrow C + 2H_2, \quad \Delta H^{\circ}_{298\,K} = 122.3\,kJ/mol \tag{4}$$

$$\text{Boudouard} \qquad 2CO \leftrightarrow C + CO_2, \quad \Delta H^{\circ}_{298\,K} = -125.2\,kJ/mol \tag{5}$$

$$\text{CO reduction} \qquad CO + H_2 \leftrightarrow C + H_2O, \quad \Delta H^{\circ}_{298\,K} = -84.0\,kJ/mol \tag{6}$$

These reactions are reversible, that is simultaneous carbon formation and gasification occur.

When CO_2 is available in large quantities and at low costs, it can be used to replace the steam partially (mixed reforming) or totally (dry reforming). The mixed reforming allows obtaining synthesis gas with different H_2/CO ratios and consequently it can be applied in many chemical and petrochemical processes. However, the presence of CO_2 augments the risk of carbon formation [2], as it produces large amounts of CO and a substantial H_2 consumption through the reverse of the water–gas-shift reaction (Eq. (2)).

An alternative to increase the methane conversion is the membrane reactor, in which the chemical equilibrium is shifted

* Corresponding author. Tel.: +54 291 4861700x210; fax: +54 291 4861600.
E-mail address: dborio@plapiqui.edu.ar (D.O. Borio).

1385-8947/$ – see front matter © 2007 Elsevier B.V. All rights reserved.
doi:10.1016/j.cej.2007.03.051

Nomenclature

Cp_j	heat capacity of component j (J/mol K)
d_p	equivalent diameter of the catalyst pellet (momentum equation) (m)
D_j^e	effective diffusivity of component j (m^2/s)
f	friction factor
F_j	molar flow rate of component j (mol/s)
ΔH_i	heat of reaction i, $i = 1, 2, 3$ (J/mol)
J_{H_2}	molar permeation flux (mol/m^2 s)
p_j	partial pressure of component j at the gas phase (Pa)
$p_{s,j}$	partial pressure of component j inside the catalyst particle (Pa)
p_t	total pressure (Pa)
r	$= \xi/(d_{cat}/2)$, dimensionless catalyst coordinate
$r_{c,net}$	net rate of carbon formation (mol_C/kg_{cat} s)
r_i	rate of the reaction i, $i = 1, 2, 3$ (mol/kg_{cat} s)
R	universal gas constant (J/mol K)
T_g	gas temperature (K)
u_s	superficial velocity (m_f^3/m_r^2 s)
V	volume of the catalyst particle (m^3)
X_{CH_4}	methane conversion
z	axial reactor coordinate (m)

Greek letters

η_i	effectiveness factor for reaction i, $i = 1, 2, 3$
$\nu_{j,i}$	stoichiometric coefficient of component j in reaction i
ξ	radial coordinate of the catalyst particle (m)
ρ_B	bed density (kg_{cat}/m_r^3)
ρ_g	gas density (kg/m_f^3)
Ω	cross sectional area of the annular catalyst bed (m_r^2)

Superscripts

0	at the reactor inlet
CR	conventional reactor
eq	at equilibrium conditions
MR	membrane reactor
p	on the permeation side
r	on the reaction side
s	at the catalyst particle surface

through preferential or selective permeation of reaction products. The removal of hydrogen from the reaction system may be performed through dense selective membranes of palladium or its alloys. However, the low permeability of these dense membranes together with the high palladium costs, have restricted their use to small-scale processes. Composed membranes constitute an adequate choice due to their high permeation flows and selectivity [3–5]. These membranes consist of a high porous substrate with low resistance to flux, covered by a metallic layer that provides the required selectivity.

In several modeling works the advantages of the membrane reactor (MR) with respect to the conventional fixed bed reactor (CR) in the methane reforming process have been demonstrated. Oklany et al. [6], Barbieri and Di Maio [7] and Galluci et al. [8] proposed 1D isothermal models to simulate the performance of membrane reactors containing Pd-based membranes. In order to study the energy transport in Pd-based membrane reactors, 1D non-isothermal models were also proposed [9,10]. To our knowledge, most of the previous works related to modeling of methane reforming in MRs have assumed negligible intraparticle mass-transfer resistances. Johannessen and Jordal [11] used a constant value of the effectiveness factor for all the reactions to simulate a catalytic membrane reactor.

The removal of hydrogen from the product stream tends to augment the risk of carbon formation by methane cracking (reaction (4)). This may affect the catalyst activity and stability, limiting the benefits of using membrane reactors for methane reforming. Hou et al. [12] evaluated the influence of hydrogen removal on the carbon formation phenomenon in a membrane reactor by means of a thermodynamic criterion based on the affinity concept for the methane cracking reaction. Although this criterion helps to identify and define conditions for the potential carbon formation by methane cracking, it results too conservative. In fact, it excludes all those operating conditions that would not lead to net carbon deposition because the rate of gasification by one of the reactions exceeds the rate of formation by the other ones [13]. Definitely this is not just a thermodynamic problem and hence kinetic aspects have to be taken into consideration [13,14].

In this work, the risk of carbon formation for a MR is kinetically analyzed and compared with that corresponding to a CR by means of a 1D heterogeneous non-isothermal model.

2. Mathematical model

Fig. 1 shows a scheme of the membrane reactor under study. It consists of two concentric tubes, an external shell installed in an electric furnace and an internal membrane tube. The membrane consists of a dense Pd layer on a porous ceramic support. The Ni catalyst is packed in the annular space and a co-current flow configuration is supposed on both sides of the membrane.

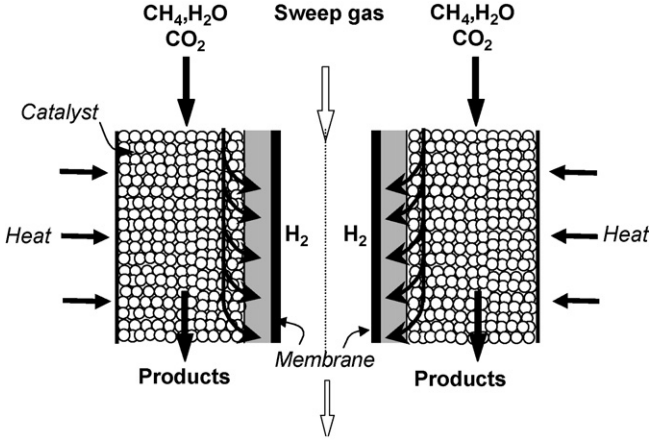

Fig. 1. Scheme of the membrane reactor for methane reforming.

In order to represent the steady-state operation of the MR, a one-dimensional heterogeneous model is adopted subject to the following assumptions:

(a) Plug-flow for the reaction and permeation sides [4,5,7,9,11,12,15].
(b) Negligible gas–solid mass and heat-transfer resistances [12].
(c) Isothermal catalyst particle [15].
(d) Isothermal and isobaric conditions for the permeate side [5,7,12].
(e) Ideal membrane (infinite selectivity to H_2) [9–11].

From these assumptions, the governing equations for the reaction and permeation side are given below

2.1. Reaction side

2.1.1. Gas phase

- Mass balances:

$$\frac{dF_j^r}{dz} = \Omega\rho_B \sum_{i=1}^{3} \eta_i r_i^s \nu_{j,i}, \quad j = CH_4, H_2O, CO, CO_2 \tag{7}$$

$$\frac{dF_{H_2}^r}{dz} = \Omega\rho_B \sum_{i=1}^{3} \eta_i r_i^s \nu_{H_2,i} - \pi\, d_{te} J_{H_2} \tag{8}$$

- Energy balance:

$$\sum_j F_j^r Cp_j \frac{dT_g^r}{dz} = \Omega\rho_B \sum_{i=1}^{3} (-\Delta H_i) r_i^s \eta_i + \pi d_{si} U (T_w - T_g^r) \tag{9}$$

- Momentum equation:

$$\frac{dp_t}{dz} = -\frac{f\rho_g u_s^2}{d_p} \tag{10}$$

- Boundary conditions:

$$\text{At } z = 0: \qquad F_j^r = F_j^0, \quad T_g^r = T_g^0, \quad p_t = p_t^0 \tag{11}$$

2.1.2. Catalyst particle

At each axial position, the internal mass-transfer resistances are accounted for by the solution of the following material balances within the catalyst particle

$$D_j^e \frac{1}{\xi}\frac{d}{d\xi}\left(\xi \frac{dp_{s,j}}{d\xi}\right) = RT_g^r \rho_p \sum_{i=1}^{3} r_i(p_{s,j}) \nu_{j,i},$$

$$j = CH_4, H_2O, CO, CO_2, H_2 \tag{12}$$

- Boundary conditions:

$$\text{at } \xi = 0: \qquad p_{s,j} = p_j^r \tag{13}$$

$$\text{at } \xi = \frac{d_{cat}}{2}: \qquad \frac{dp_{s,j}}{d\xi} = 0 \tag{14}$$

The intrinsic kinetics reported by Xu and Froment [16] is selected for reactions (1)–(3). The effective diffusivities are calculated using the expressions given by Xu and Froment [17].

2.2. Permeation side

- Mass balances:

$$\frac{dF_{sweep}^p}{dz} = 0 \tag{15}$$

$$\frac{dF_{H_2}^p}{dz} = \pi d_{te} J_{H_2} \tag{16}$$

- Boundary conditions:

$$\text{At } z = 0: \qquad F_{sweep}^p = F_{sweep}^0, \quad F_{H_2}^p = 0 \tag{17}$$

The hydrogen permeance through the membrane is evaluated using the Sievert law [10,11]:

$$J_{H_2} = \frac{Q_0\, e^{-E_p/RT_g^r}}{\delta}\left[\sqrt{p_{H_2}^r} - \sqrt{p_{H_2}^p}\right] \tag{18}$$

where δ is the membrane thickness and $p_{H_2}^r$ and $p_{H_2}^p$ are the hydrogen partial pressures on the reaction and permeation sides, respectively.

2.3. Numerical solution

The differential equations for the gas phase on reaction and permeation sides are integrated by means of a GEAR routine [18]. The differential equations for the particle are discretized by means of second order finite differences, using an adaptive grid of two elements with variable width. Forty and five grid points are assigned to the first (near the catalyst surface) and second element, respectively. For each axial position, the 98 resultant non-linear algebraic equations are solved through a Quasi Newton algorithm. Once the partial pressures for all the components are obtained ($p_{s,j}$), the effectiveness factors for reactions (1)–(3) are calculated through Eq. (19).

$$\eta_i = \frac{\int_0^V r_i(p_{s,j})(dV/V)}{r_i(p_j^r)}, \quad i = 1, 2, 3,$$

$$j = CH_4, H_2O, CO, CO_2, H_2 \tag{19}$$

The trends of the main variables predicted by the above-presented MR model were validated against experimental and numerical results from the literature [9–11].

The net rate of carbon deposition (reactions (4)–(6)) is evaluated by means of the following kinetic expression reported by Snoeck et al. [13]:

$$r_{c,net} = \frac{r_{c,4} + r_{c,(5+6)}}{DEN^2} \tag{20}$$

where:

$$r_{c,4} = k_M^+ K_{CH_4}\left(p_{CH_4} - \frac{1}{K_{M,av}^*}\, p_{H_2}^2\right) \tag{21}$$

$$r_{c,(5+6)} = k_O^{+'} \left(K_{O,H_2O} \frac{K_1}{K^*_{M,av}} p_{CO} - \frac{1}{K_{O,H_2O}} \frac{p_{H_2O}}{p_{H_2}} \right) \quad (22)$$

$$DEN = 1 + K_{CH_4} p_{CH_4} + \frac{1}{K''_r} p_{H_2}^{3/2} + \frac{1}{K_{O,H_2O}} \frac{p_{H_2O}}{p_{H_2}} \quad (23)$$

The term $r_{c,4}$ of Eq. (20) represents the carbon formation by CH_4 cracking and its gasification by H_2 (reaction (4)), while $r_{c,(5+6)}$ groups the carbon formation by reactions (5) and (6), and its gasification by CO_2 and H_2O. The values of the coefficients involved in Eqs. (21)–(23) can be found in [13].

The net rate of carbon formation has been assumed everywhere negligible with respect to the main reaction rates. For this reason, once the model is solved and the gas composition and temperature profiles are known, the $r_{c,net}$ expression is used to calculate the potential of carbon formation at each axial position and inside the catalyst. According to the kinetic criterion, if $r_{c,net} \geq 0$ at any position along the reactor, carbon deposition occurs [13].

3. Results and discussion

The performance of the MR was compared with that of a CR, which was modeled by assuming null H_2 permeation. The geometric parameters and operating conditions used in the simulations of the CR and MR are given in Table 1.

The influence of the feed CO_2 and H_2O contents on carbon formation in the CR and MR is shown in Fig. 2. For each reactor configuration, the curve represents the boundary between carbon-forming and carbon-free regions for different feed compositions. For both reactor designs, as the CO_2 feed content is increased higher H_2O/CH_4 ratios are required to avoid carbon deposition. However, more steam has to be added in the case of MR (i.e., the range of feed conditions leading to carbon formation is wider). For each of the operating conditions presented in Fig. 2, the conversion for the MR is higher than that of the CR and even higher than the corresponding equilibrium value. These results suggest a trade-off between higher production rates and higher risk of carbon formation.

Table 1
Geometric parameters and operating conditions used to simulate the CR and MR

Parameter	Value
Reactor length, L	0.2 m [9]
Shell internal diameter, d_{si}	0.0326 m [9]
Tube internal diameter, d_{ti}	0.021 m [9]
Tube external diameter, d_{te}	0.025 m [9]
Catalyst mass/reactor length, W/L	0.05 kg/m [9]
Bed porosity, ε_B	0.5 [11]
Catalyst	30% Ni/Al_2O_3 [9]
Diameter of the catalyst particle, d_{cat}	0.001 m [10]
Height of the catalyst particle, h_{cat}	0.003 m [10]
Particle density, ρ_p	2355.3 kg/m^3 [11]
Thickness of Pd film, δ	7.5 μm [9]
Pre-exponential factor of the Sievert permeability coefficient, Q_0	6.3×10^{-4} mol s^{-1} m^{-1} MPa$^{1/2}$ [11]
Activation energy of the hydrogen permeability, E_p	15700 J/mol [11]
Overall heat transfer coefficient, U	227 W/m^2 K [9]
Tube-wall temperature, T_w	500 °C [9]
Methane feed volumetric flow rate, $Q^0_{CH_4}$	200 sccm [9]
Feed temperature, T^0_g	500 °C [9]
Feed pressure, p^0_g	100 kPa [9]
Sweep gas temperature, T_{sweep}	500 °C [9]
Sweep gas volumetric flow rate, Q^0_{sweep}	2000 sccm [9]
Sweep gas pressure, P_{sweep}	100 kPa [9]

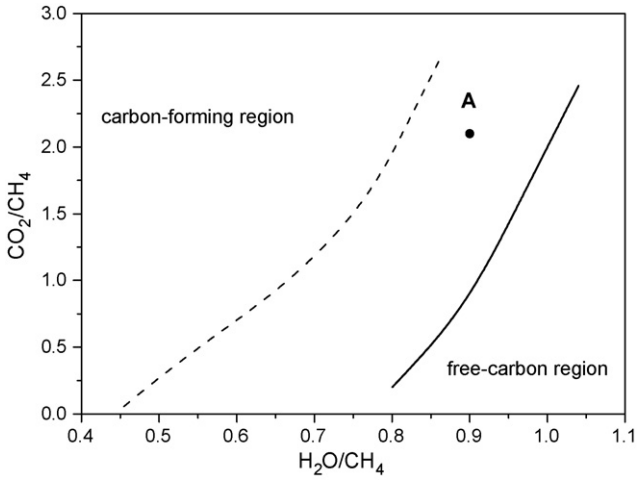

Fig. 2. Influence of the H_2O/CH_4 and CO_2/CH_4 ratios on carbon formation in the CR (dashed line) and MR (full line).

In order to compare the carbon deposition phenomenon in both reactors, Fig. 3 shows (for the feed condition A of Fig. 2) the $r_{c,net}$ curves along the reactor length, at the catalyst surface ($r=0$) and catalyst center ($r=1$). As it can be seen, no carbon formation takes place in the CR ($r_{c,net}<0$) while in the MR carbon deposition is predicted from the critical axial position $z_c = 0.117$ m towards the reactor outlet.

This behavior can be explained by means of Fig. 4, in which the axial composition profiles for both reactors are presented. The diminution in p_{H_2} caused by the H_2 permeation through the membrane increases the rate of carbon deposition by CH_4

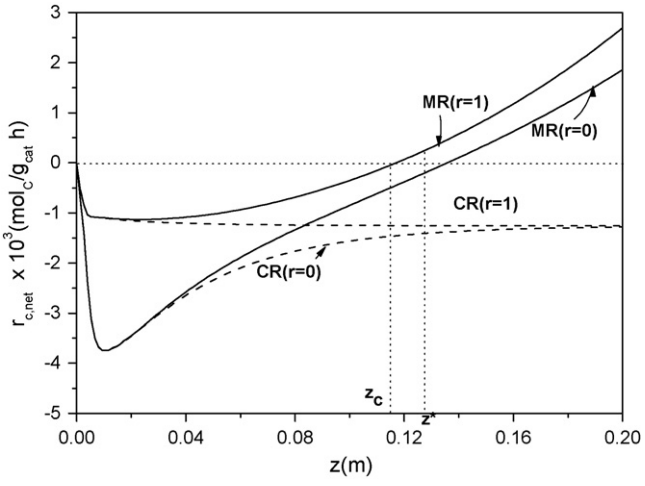

Fig. 3. Axial profiles of the net carbon deposition rate in the CR and MR (condition A of Fig. 2). $r=0$: catalyst surface; $r=1$: catalyst center.

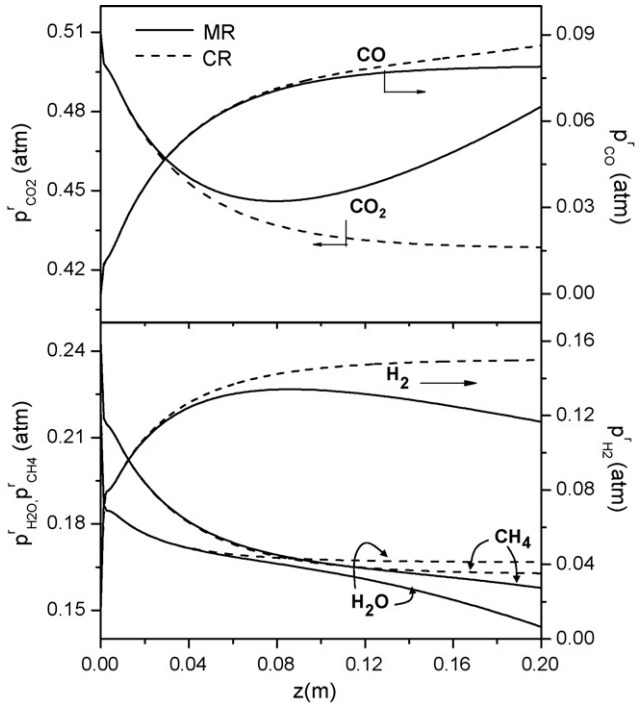

Fig. 4. Axial variation of composition for the CR and MR (condition A of Fig. 2).

cracking (reaction (4)). Besides, p_{H_2O} is lower for the MR as a consequence of the higher CH_4 conversion and the shift to the right of the WGS reaction (2). The shift of reaction (2) towards products, caused by the hydrogen permeation, is also expressed through the minimum observed in the CO_2 curve. Thus, the outlet conversion of the reactant CO_2 is clearly lower in the MR.

Even though p_{H_2} and p_{CO} are lower in the MR, the lower p_{H_2O} values promote carbon formation also by CO reduction (reaction (6)), i.e. $r_{c,(5+6)}$ becomes positive towards the reactor outlet. Since the axial temperature profiles for both reactors are very similar (results not shown in this work), it is not possible to attribute the differences observed in $r_{c,net}$ to a thermal effect.

As shown in Fig. 3, the $r_{c,net}$ values at the particle center ($r = 1$) are higher than those corresponding to the catalyst surface ($r = 0$) for both reactors. This particular result can be explained by analysis of Figs. 5 and 6. For the case of the MR, Fig. 5 shows the rates of carbon formation within the catalyst particle at $z^* = 0.128$ m (see also Fig. 3). From the catalyst surface and up to $r \cong 0.005$, the rate of carbon deposition by reaction (4) is lower than the rate of carbon gasification by reactions (5) and (6), thus $r_{c,net}$ is negative (see Eq. (20)).

From $r \cong 0.005$ to the particle center, the model predicts carbon formation ($r_{c,net} > 0$), as a consequence of the composition gradients calculated inside the catalyst (see Fig. 6). The decrease in p_{CH_4} and the increase in p_{H_2} along the radial coordinate cause the diminution in $r_{c,4}$ values shown in Fig. 5. However, the increment in p_{CO} and the decrement in p_{H_2O} are responsible for the continuous augment in the $r_{c,(5+6)}$ curve and consequently in the $r_{c,net}$ curve. Once chemical equilibrium conditions are reached (for $r > 0.04$), the $r_{c,net}$ curve keeps constant at a positive value.

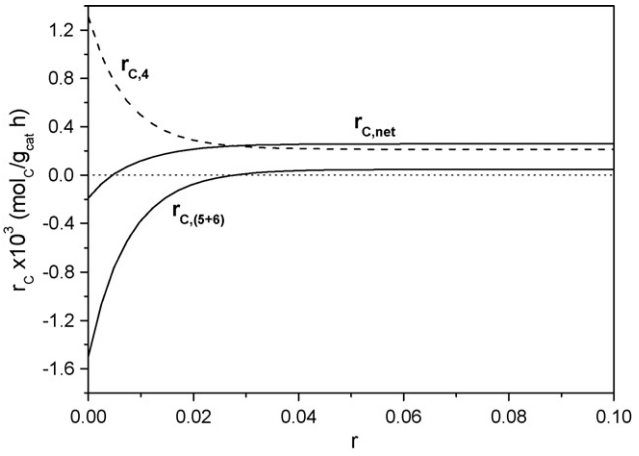

Fig. 5. Profiles of $r_{c,net}$, $r_{c,4}$ and $r_{c,(5+6)}$ within the catalyst at $z^* = 0.128$ m for the MR (condition A of Fig. 2).

The results shown in Figs. 5 and 6 demonstrate the importance of taking into account the intraparticle diffusional limitations to evaluate the risk of carbon formation in MRs. In fact, for the considered Ni catalyst and high CO_2 contents in the feed, the highest risk of carbon deposition is detected at the center of the catalyst particle.

The influence of the membrane thickness on the carbon deposition and the methane conversion is shown in Fig. 7. The risk of carbon deposition increases as the membrane thickness is lowered, i.e. as higher permeation rates of hydrogen take place. For the analyzed operating conditions, the lowest membrane thickness leads to the highest methane conversion, but also to the highest risk of carbon formation.

The effect of the tube-wall temperature on the carbon formation phenomenon is presented in Fig. 8. It is clear that the temperature increase at the tube-wall (and consequently in the process gas) tends to favor carbon deposition. For the selected operating conditions, the lowest temperature ($T_w = 480\,^\circ$C) leads to carbon-free conditions along over 80% of the total reactor length, whereas for $T_w = 540\,^\circ$C almost all the reactor length is affected by carbon formation.

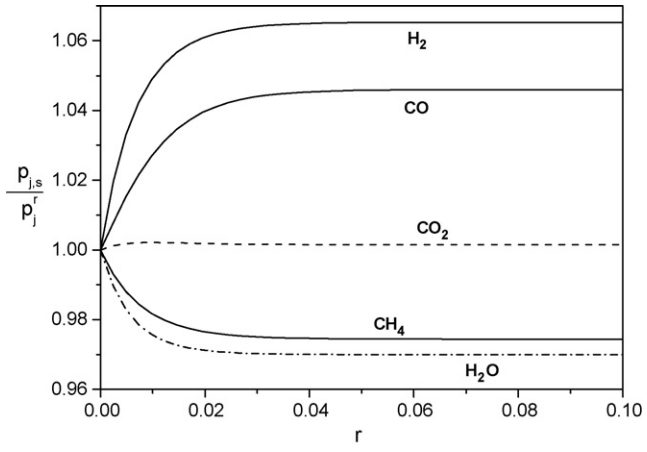

Fig. 6. Partial pressures (dimensionless values) within the catalyst particle at $z^* = 0.128$ m for the MR (condition A of Fig. 2).

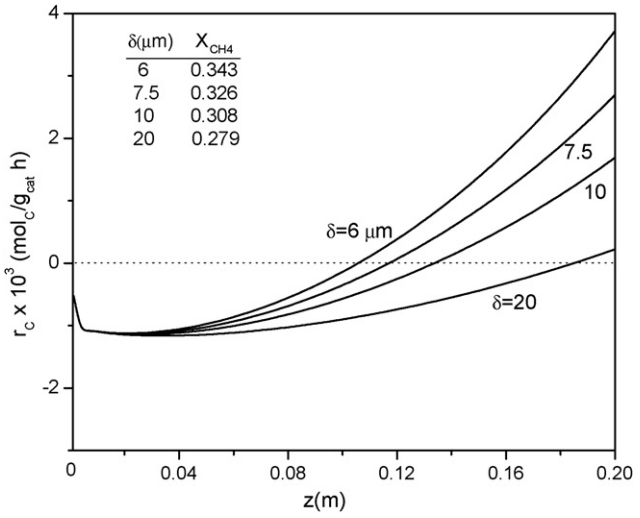

Fig. 7. Axial profiles of the net carbon deposition rate in the MR (condition A of Fig. 2), at the center of the catalyst particle ($r = 1$) and for different membrane thickness.

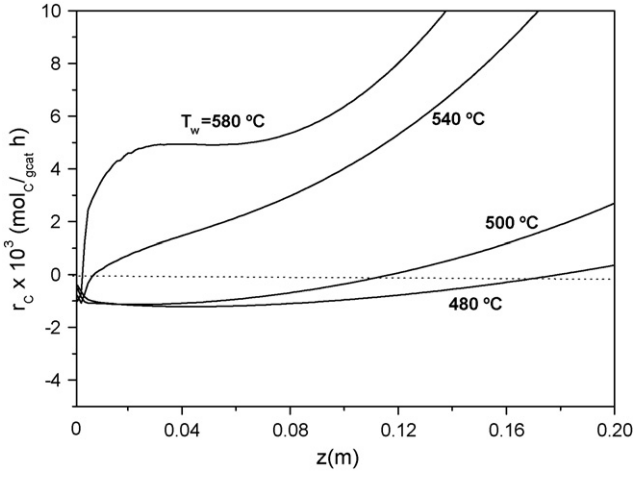

Fig. 8. Axial profiles of the net carbon deposition rate in the MR (condition A of Fig. 2), at the center of the catalyst particle ($r = 1$) and for different tube-wall temperatures.

At this point, it is convenient to remark the importance of a correct evaluation of the internal mass-transfer resistances. Despite the relatively low temperatures for which the MR is being simulated, the calculated effectiveness factors are noticeably low. For the conditions of Fig. 8, the effectiveness factor corresponding to the reforming reaction (1) varies between $\eta_1 = 0.008$ (at $T_w = 580\,^{\circ}C$) and 0.015 (at $T_w = 480\,^{\circ}C$). Regarding reaction (3), typical values for η_3 are around 0.007 (at $T_w = 580\,^{\circ}C$) and 0.014 (at $T_w = 480\,^{\circ}C$).

4. Conclusions

A comparative kinetic analysis of the carbon deposition phenomenon on a Ni catalyst in the CR and MR has demonstrated that carbon formation is favored when the CO_2 content in the feed or the operating temperature increases. The risk of carbon deposition should be carefully evaluated along the reactor, not only at the catalyst surface but also within the particle, by considering simultaneously the three possible sources of carbon formation (reactions (4)–(6)).

The hydrogen permeation through the membrane increases the risk of carbon formation and the methane conversion with respect to those of the conventional fixed bed reactor. Therefore, the selection of the membrane thickness becomes a trade-off between the improvement in the reactor performance and the higher potential for carbon formation.

The quantification of the composition gradients inside the catalyst particle is useful not only to take into account the strong internal mass-transfer resistances (i.e., to avoid an overestimation of the observed reaction rates), but also to detect the positions where the risk of carbon deposition becomes maximum. For the case of methane reforming with CO_2 (or feeds with high CO_2/H_2O ratios), the highest risk of carbon formation is located at the particle center.

Acknowledgement

The financial contribution of CONICET (Argentina) is gratefully acknowledged.

References

[1] J.R. Rostrup Nielsen, Catalytic steam reforming, Catal. Sci. Technol. 1 (1984) 1.
[2] A.M. De Groote, G.F. Froment, Reactor modeling and simulation in synthesis gas production, Rev. Chem. Eng. 11 (1995) 145.
[3] W.-H. Lin, H.-F. Chang, Characterization of Pd–Ag membrane prepared by sequential electroless deposition, Surf. Coat. Technol. 194 (2005) 157.
[4] E. Kikuchi, Y. Nemoto, M. Kajiwara, S. Uemiya, T. Kojima, Steam reforming of methane in membrane reactors: comparison of electroless-plating and CVD membranes and catalyst packing modes, Catal. Today 56 (2000) 75.
[5] J. Shu, B.P.A. Grandjean, S. Kaliaaguine, Methane steam reforming in asymmetric Pd- and Pd-Ag/porous SS membrane reactors, Appl. Catal. A: Gen. 119 (1994) 305.
[6] J.S. Oklany, K. Hou, R. Hughes, A simulative comparison of dense and microporous membrane reactors for the steam reforming of methane, Appl. Catal. A: Gen. 170 (1998) 13.
[7] G. Barbieri, F.P. Di Maio, Simulation of methane steam reforming process in a catalytic Pd-membrane reactor, Ind. Eng. Chem. Res. 36 (1997) 2121.
[8] F. Gallucci, L. Paturzo, A. Basile, A simulation study of the steam reforming of methane in a dense tubular membrane reactor, Int. J. Hydrogen Energ. 29 (2004) 611.
[9] G. Marigliano, G. Barbieri, E. Drioli, Effect of energy transport on a palladium-based membrane reactor for methane steam reforming process, Catal. Today 67 (2001) 85.
[10] G. Madia, G. Barbieri, E. Drioli, Theoretical and experimental analysis of methane steam reforming in a membrane reactor, Can. J. Chem. Eng. 77 (1999) 698.
[11] E. Johannessen, K. Jordal, Study of H_2 separating membrane reactor for methane steam reforming at conditions relevant for power processes with CO_2 capture, Energ. Convers. Manage. 46 (2005) 1059.
[12] K. Hou, M. Fowles, R. Hughes, Potential catalyst deactivation due to hydrogen removal in a membrane reactor used for methane steam reforming, Chem. Eng. Sci. 54 (1999) 3783.
[13] J.-W. Snoeck, G.F. Froment, M. Fowles, Kinetic evaluation of carbon formation in steam/CO_2-natural gas reformers: influence of the catalyst activity and alkalinity, Int. J. Chem. Reactor Eng. A7 (2003) 1.

[14] J. Piña, V. Bucalá, D.O. Borio, Optimization of steam reformers: heat flux distribution and carbon formation, Int. J. Chem. Reactor Eng. A25 (2003) 1.
[15] G.F. Froment, K.B. Bischoff, Chemical Reactor Analysis and Design, John Wiley & Sons, NY, USA, 1990.
[16] J. Xu, G.F. Froment, Methane steam reforming, methanation and water–gas shift. I. Intrinsic kinetics, AIChE J. 35 (1989) 88.
[17] J. Xu, G.F. Froment, Methane steam reforming. II. Diffusional limitations and reactor simulation, AIChE J. 35 (1989) 98.
[18] L.F. Shampine, C.W. Gear, SIAM Rev. 21 (1979) 1.